JACS
JOURNAL OF THE AMERICAN CHEMICAL SOCIETY
Article
pubs.acs.org/JACS

Spin Isomers and Ligand Isomerization in a Three-Coordinate Cobalt(I) Carbonyl Complex

Malik H. Al-Afyouni,[†] Elizaveta Suturina,[‡,⊥] Shubhrodeep Pathak,[‡] Mihail Atanasov,[‡,§] Eckhard Bill,[‡] Daniel E. DeRosha,[∥] William W. Brennessel,[†] Frank Neese,[‡] and Patrick L. Holland*[,†,∥]

[†]Department of Chemistry, University of Rochester, Rochester, New York 14618, United States
[‡]Max Planck Institute for Chemical Energy Conversion, Stiftstrasse 32-34, D-45470 Mülheim an der Ruhr, Germany
[§]Institute of General and Inorganic Chemistry, Bulgarian Academy of Sciences, Akademy Georgi Bontchev Street 11, 1113 Sofia, Bulgaria
[∥]Department of Chemistry, Yale University, New Haven, Connecticut 06520, United States
[⊥]Novosibirsk State University, Pirogova Street 2, 630090 Novosibirsk, Russia

Supporting Information

ABSTRACT: Hemilabile ligands, which have one donor that can reversibly bind to a metal, are widely used in transition-metal catalysts to create open coordination sites. This change in coordination at the metal can also cause spin-state changes. Here, we explore a cobalt(I) system that is poised on the brink of hemilability and of a spin-state change and can rapidly interconvert between different spin states with different structures ("spin isomers"). The new cobalt(I) monocarbonyl complex L^{tBu}Co(CO) (**2**) is a singlet (^{1}**2**) in the solid state, with an unprecedented diketiminate binding mode where one of the C═C double bonds of an aromatic ring completes a pseudo-square-planar coordination. Dissolving the compound gives a substantial population of the triplet (^{3}**2**), which has exceptionally large uniaxial zero-field splitting due to strong spin−orbit coupling with a low-lying excited state. The interconversion of the two spin isomers is rapid, even at low temperature, and temperature-dependent NMR and electronic absorption spectroscopy studies show the energy differences quantitatively. Spectroscopically validated computations corroborate the presence of a low minimum-energy crossing point (MECP) between the two potential energy surfaces and elucidate the detailed pathway through which the β-diketiminate ligand "slips" between bidentate and arene-bound forms: rather than dissociation, the cobalt slides along the aromatic system in a pathway that balances strain energy and cobalt−ligand bonding. These results show that multiple spin states are easily accessible in this hemilabile system and map the thermodynamics and mechanism of the transition.

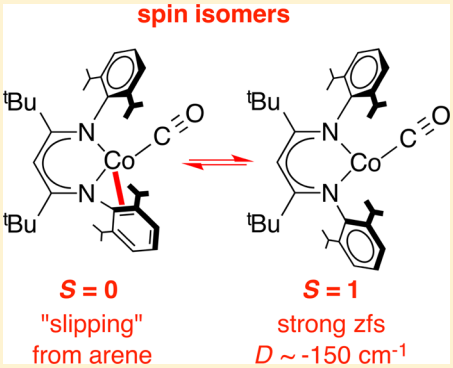

INTRODUCTION

Stoichiometric and catalytic reactions of transition metals often require an open coordination site at the metal, but these unsaturated species can be unstable. Thus, substantial research effort has gone into the design of "hemilabile" ligands, which are chelating supporting groups in which one of the donors can easily break its bond to the metal and generate the open site needed for a reaction (Figure 1).[1−3] For example, hemilabile ligands have been used in catalytic olefin polymerization, Suzuki−Miyaura coupling reactions, and hydrogenation reactions.[4−7]

However, hemilability can reversibly modify other aspects of a metal site as well. For example, the spin state of complexes is intimately connected to the ligand field and the coordination number. Therefore, a hemilabile ligand could allow access to multiple spin states through reversible dissociation. Lowering the activation barrier for a reaction by shifting between spin states, termed "spin acceleration" by Poli and "two-state reactivity" by Shaik, is increasingly recognized as a way to facilitate bond-breaking and bond-forming reactions of inexpensive first-row transition-metal complexes.[8−11] However, the links between reversible ligand lability and reversible spin-state changes have rarely been examined in detail.[12−16]

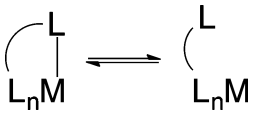

Figure 1. Hemilabile ligands reversibly dissociate one donor from the metal. In addition to creating an open coordination site for reactivity, the change in coordination could potentially change the geometry and thus the spin state of the metal center.

In order to evaluate this opportunity using a well-characterized, accessible system, we explore here the chemistry of cobalt complexes supported by the β-diketiminate ligand

Received: June 11, 2015
Published: August 12, 2015

DOI: 10.1021/jacs.5b06078
J. Am. Chem. Soc. 2015, 137, 10689−10699

2,2,6,6-tetramethyl-3,5-bis(2,6-diisopropyl-phenylimido)hept-4-yl (abbreviated L^{tBu}). Though β-diketiminates are typically bidentate, binding through the two N atoms, we have shown that $L^{tBu}Co(THF)$ reversibly loses a weakly bound tetrahydrofuran (THF) ligand, accompanied by a shift of the supporting ligand that dissociates one of the nitrogen donors and coordinates an arene ring to give $L^{tBu}Co$ (**1** in Scheme 1).[17]

Scheme 1. Rearrangement of the Diketiminate Ligand in $L^{tBu}Co$ (1) to the Bidentate Form upon Coordination of Lewis Bases THF, PPh_3, Pyridine, or CO[17]

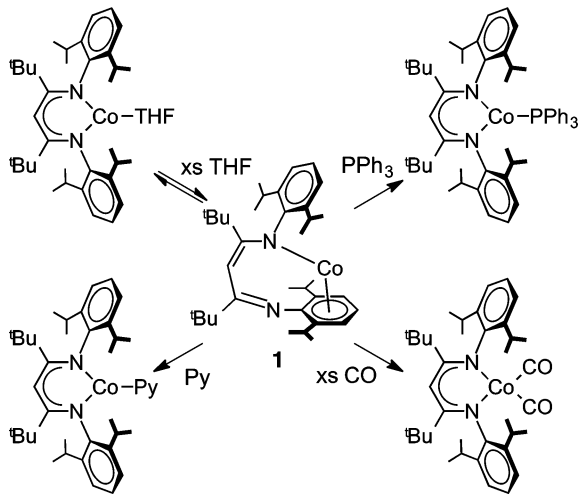

Thus, the hemilabile diketiminate ligand enables the complex to avoid the formation of a 12-electron, two-coordinate cobalt(I) species by binding the arene to achieve a 16-electron configuration. Addition of Lewis bases (CO, PPh_3, pyridine) to $L^{tBu}Co$ makes the β-diketiminate ligand rearrange rapidly back to its customary bidentate form (Scheme 1). Interestingly, this system shows rapid reversibility of ligand association/dissociation despite a large change in the ligand geometry. The ligand rearrangement also enables $L^{tBu}Co$ to perform difficult reactions such as C−F bond cleavage.[17,18]

The previous studies raised deep questions about the rearrangement, the answers to which would teach general lessons of use for the rational design of supporting ligands that give reversible spin-state changes. First, kinetic studies did not clarify whether coordination of the added ligand and isomerization of the supporting ligand were concurrent or occurred in a stepwise fashion. Second, the rapid reaction of $L^{tBu}Co$ with CO involves a spin flip from triplet $L^{tBu}Co$ to singlet $L^{tBu}Co(CO)_2$, despite the possibility of a "spin barrier" as observed in related Fe complexes.[9,19−21] Here, we describe a comprehensive study that answers these questions using synthesis, spectroscopy, crystallography, magnetism, and both density functional and ab initio computations. These studies center around a novel three-coordinate cobalt(I) carbonyl complex, $L^{tBu}Co(CO)$, which undergoes rapid spin crossover and ligand isomerization in solution. In the course of these studies, we also show that the high-spin form of $L^{tBu}Co(CO)$ has unusually large magnetic anisotropy. Comparative analysis of the magnetism of $L^{tBu}Co$ and $L^{tBu}Co(CO)$ combined with ab initio ligand field study elucidates the nature of the zero-field splitting of the high-spin $L^{tBu}Co(CO)$ that gives these magnetic properties.

RESULTS

Synthesis and Characterization of $L^{tBu}Co(CO)$ (2). The addition of **1** to an equimolar solution of the dicarbonyl complex $L^{tBu}Co(CO)_2$ in pentane gives $L^{tBu}Co(CO)$ (**2**, Scheme 2). This comproportionation reaction proceeds rapidly and quantitatively at room temperature and yields red single crystals of **2** that are suitable for X-ray crystallography.

Scheme 2. Synthesis of $L^{tBu}Co(CO)$ (2)

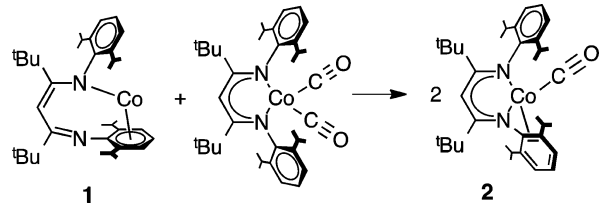

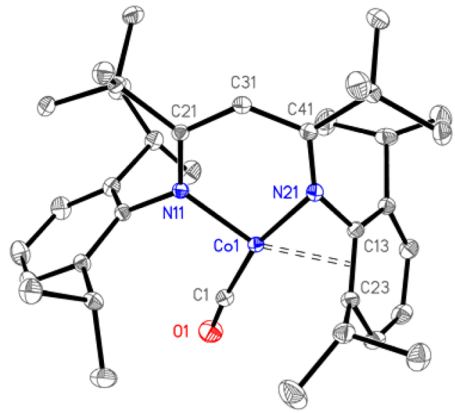

Figure 2. Crystal structure of $L^{tBu}Co(CO)$ (**2**). Thermal ellipsoids are shown at 50% probability. H atoms are omitted for clarity. Co1−C1 = 1.743(1) Å, Co1−N11 = 1.9019(9) Å, Co1−N21 = 1.811(1) Å, Co1−C13 = 2.041(1) Å, Co1−C23 = 2.220(1) Å, C1−O1 = 1.154(2) Å, N21−Co1−N11 = 94.50(4)°, C1−Co1−N11 = 101.86(5)°, C(13−23)*−Co1−C1 = 108.41(4)°, C(13−23)*−Co1−N21 = 55.29(4)°, Co1−C1−O1 = 174.3(1)°. Asterisk (*) indicates the calculated centroid.

The crystallographic structure of **2** (Figure 2) shows that it has a previously unknown binding mode of the β-diketiminate ligand,[22] in which the binding of both N atoms is accompanied by an η^2 interaction with one of the aryl groups. In the η^2-bound arene, there is shortening of two localized double bonds with short C−C distances of C33−C43 = 1.357(2) Å and C53−C63 = 1.366(2) Å, and the C−C bond that interacts with the Co center (C13−C23 = 1.435(2) Å) is significantly longer than the corresponding C−C bond of the unbound arene ring (C12−C62 = 1.404(2) Å). The bond between the N and the ipso carbon of the η^2-bound arene is anomalously short (1.389(1) vs 1.451(1) Å for the N−C^{ipso} for the other arene), suggesting that it is possible to view the bonding as a π-azaallyl interaction to one side of the diketiminate. However, in contrast to **1**, which has π-bond localization in the diketiminate N_2C_3 backbone, **2** has a delocalized backbone with fairly similar C−N (1.345(1) and 1.323(2) Å) and C−C (C21−C31 = 1.418(2) and 1.385(2) Å) bond lengths. Thus, in **2** the backbone of the diketiminate is much like that in the κ^2-*N,N′* form, while the main distortion is in the arene that binds η^2 to the metal, which gains some π-azaallyl character.

DOI: 10.1021/jacs.5b06078
J. Am. Chem. Soc. 2015, 137, 10689−10699

The arene ring is dramatically tilted toward the Co center as judged by the small Co−N−C_{Ar} angle of 78.04(6)° (Co−N−C_{Ar} angle for unbound arene ring = 114.26(7)°). Considering the centroid of the bound C═C bond as a single donor to the metal, the geometry at the cobalt(I) center may be described as distorted square planar, with a sum of 360.06(9)° for the angles around Co. In **2**, the CO ligand is nearly linear (Co−C−O = 174.3(1)°) with a bond length of 1.154(2) Å.

The infrared (IR) spectrum of red solid **2** (Figure 3, red) shows a strong CO stretching vibration at 1938 cm^{-1}.

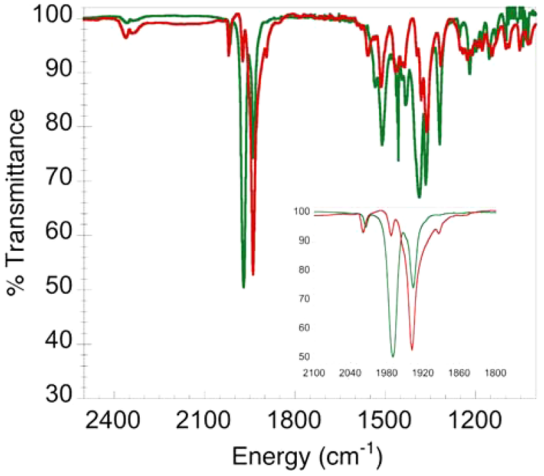

Figure 3. IR spectra of **2** as a solid (red) and benzene solution (green).

Interestingly, dissolving **2** in THF or benzene gives a significant shift of the CO vibration to 1969 cm^{-1} (Figure 3 and S1, green) and a color change from red to yellow-green. The change is not complete, because the solution IR spectra of **2** consistently contain the 1938 cm^{-1} signal as well. Upon removal of solvent under vacuum, the yellow-green color reverts back to red. These variations in spectroscopic properties suggest that the solution and solid-state structures are different.

The ^{1}H NMR spectrum of **2** gives insight into the solution structure. The spectra in C_6D_6 or THF-d_8 each feature seven singlets that are paramagnetically shifted, with integrations that are consistent with C_{2v} symmetry in the complex (Figure S2). The observation of symmetry higher than that in the crystal structure, where the arene rings of the diketiminate are apparently equivalent in solution, indicates a more symmetric structure than in the solid state. Lowering the temperature of an NMR sample in THF-d_8 causes no decoalescence of peaks as low as −80 °C (Figure S3). Rather, the peaks shift away from 0 ppm, consistent with the behavior of a paramagnetic compound according to the Curie law.[23] The solution magnetic moment at room temperature (measured using the Evans method)[24] is 3.3 μ_B, which is consistent with an $S = 1$ ground state with $g_{average} \approx 2.3$. Below, we will explain the temperature-dependent NMR data in greater detail.

The magnetization of **2** was probed more directly using superconducting quantum interference device (SQUID) magnetometry on two samples: the red solid and a green-yellow solution in eicosane (4.46 wt %) that is trapped in its solution form at the solvent freezing point of 37 °C (Figure 4). The frozen solution data fit to a 69% population of an $S = 1$ species. (The $S = 1$ state is clearly indicated by the constant magnetic moment at temperatures above 100 K; the low-temperature behavior of the magnetization is due to zero-field splitting, as discussed in detail below.) The SQUID response for red solid **2** fits to an 8% population of the same $S = 1$ species; thus, the majority of the sample is diamagnetic in the solid state. Overall, our magnetic data indicate that **2** is a singlet ($S = 0$) in the red crystalline solid, and the solution NMR and magnetism indicate that it undergoes a transition to a more symmetric triplet state ($S = 1$) in solution. Because the IR data show that the structures of the two spin states are different, we shall refer to these as *spin isomers* and show computations and further spectroscopic/magnetic studies to elucidate their structures and properties below.

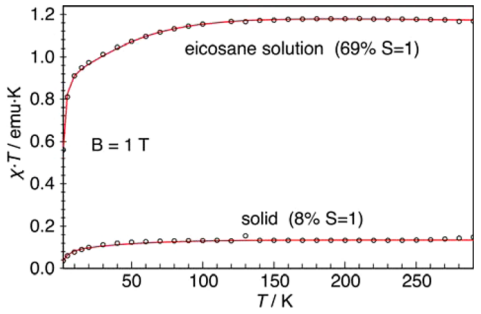

Figure 4. Solid and solution magnetic susceptibility measurements of **2**. Red lines are simulations for $S = 1$ with **g** = [2.14, 2.14, 3.24], $D = -150$ cm^{-1}, and $E/D = 0.01$ (see below).

Quantification of the Energy Difference Between Spin Isomers. The difference between the energies of the singlet and triplet forms in solution was evaluated using variable-temperature UV−vis and ^{1}H NMR spectroscopies. In the UV−vis spectra, temperature-dependent changes are evident, with a shoulder at $\lambda_{max} \approx 420$ nm growing in at low temperature and a small shoulder at $\lambda_{max} \approx 580$ nm disappearing in the same temperature range (Figure 5, red and blue solid lines). Van't Hoff plots at each wavelength (Figures S4 and S5) give the following thermodynamic parameters for ^{1}**2** to ^{3}**2**: $\Delta H = 1.6 \pm 0.8$ kcal/mol, $\Delta S = 9 \pm 3$ cal/mol·K, and $T_c = \Delta H/\Delta S \approx 180$ K.

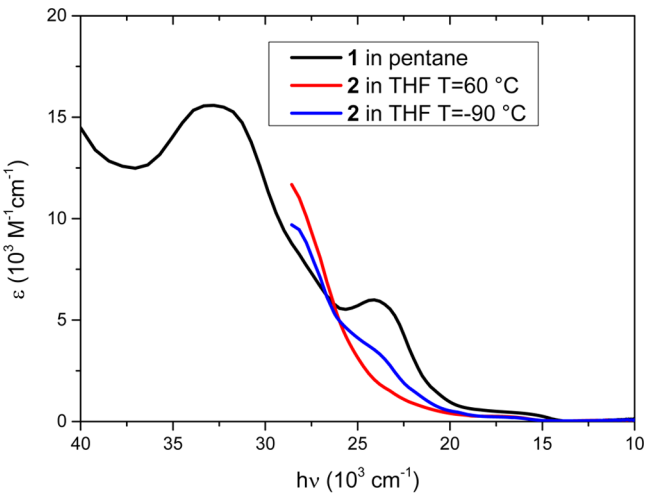

Figure 5. Comparison between electronic absorption spectra of **1** in pentane at room temperature (black) and **2** in THF at temperatures of 60 (red) and −90 °C (blue). Spectra at intermediate temperatures and van't Hoff plots are shown in Figures S4 and S5.

DOI: 10.1021/jacs.5b06078
J. Am. Chem. Soc. 2015, 137, 10689−10699

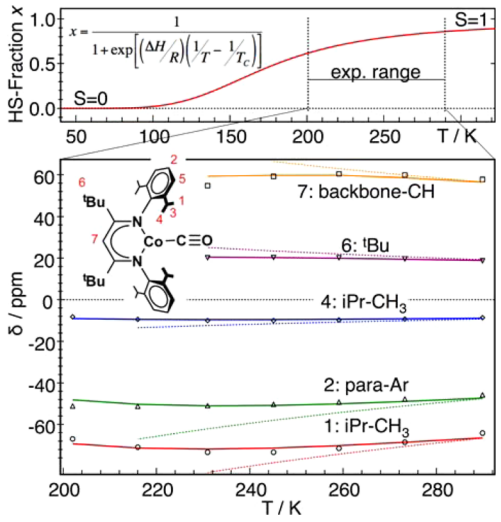

Figure 6. Temperature dependence of the paramagnetically shifted NMR resonances of **2** in THF-d_8 solution (bottom) and behavior of a $S = 0/S = 1$ spin transition (top). Solid lines in both panels are derived from a solution model for the transition[25] as described in the text with T_C = 180 K and ΔH = 601 cm^{-1} (= 1.7 kcal/mol). Diamagnetic shift values δ_0 were fixed to δ 1.2, 7.2, 1.2, 1.3, and 4.1 ppm. Dotted lines in the bottom panel illustrate the low-temperature changes expected for a hypothetical $S = 1$ species without spin crossover. Thus, the spin crossover model is required to explain the changes in chemical shift.

NMR spectroscopy enabled more direct evaluation of the changes in magnetism with temperature. Lowering the temperature of a solution in THF-d_8 caused the paramagnetically shifted resonances to move away from the diamagnetic region, as mentioned above.[23] Below −45 °C, however, lowering the temperature shifts the ^{1}H resonances of **2** back toward the diamagnetic region (Figure 6, bottom). The temperature dependence of the chemical shifts in the ^{1}H NMR spectra was simulated as a reversible transition between ^{1}**2** and ^{3}**2** in solution (Figure 6, top), where the former dominates at low temperature and the latter dominates at high temperature. In our approach, based on the usual solution model without cooperativity,[25] the fraction of high-spin molecules, $x(T) = 1/(1 + \exp[(\Delta H/R)(1/T - 1/T_c)]$, is determined by the enthalpy difference ΔH between low-spin and high-spin states (which defines the width of the transition) and the transition temperature T_c. We assume that the ligand protons have fast electronic spin relaxation and therefore experience a time- and directionally-averaged internal field that is proportional to the molar magnetization, $m(T)$, of the paramagnetic cobalt(I) ion. The magnetization in turn is governed by the competing effects of increasing high-spin fraction $x(T)$ and decreasing magnetization according to the Curie law, $m(T) \propto x(T)/T$. (The simple Curie approach is applicable here, because k_BT is larger than zero-field and Zeeman splitting of the triplet at the temperatures used in the NMR experiment.) The internal field then causes temperature-dependent shifts according to $\delta(T) = \delta_0 + \delta_p \cdot m(T)$, where δ_0 is the line position for the sample in the diamagnetic ground state ($S = 0$) and δ_p is a coefficient describing the influence of the cobalt magnetization on the chemical shift. A global fit for the five different resonances with δ_0 fixed to the chemical shifts of the protons in the free ligand yielded T_c = 180 K and ΔH = 1.7 kcal/mol (Figure 6). The values estimated for the spin-state change are similar to spin-state crossover in other iron and cobalt complexes.[25−28] Importantly, the value of ΔH from the NMR fit was close to those from van't Hoff plots from UV−vis data, indicating a self-consistent model for the interconversion of the spin isomers.

DFT Computations on 2 Give Insight into the Structural/Magnetic Differences between Spin Isomers. We investigated the structures of the two spin isomers using density-functional theory (DFT), employing the def2-TZVP basis set of Alrichs.[29] The full complex L^{tBu}Co(CO) (**2**) was used, and optimized geometries were subjected to frequency calculations that gave both vibrational frequencies for comparison to infrared spectra (Figure S6) and also entropies to derive the free energies ($\Delta G°$) of different forms. Because the optimal choice of functional was not obvious, we tested BP86,[30,31] B3LYP,[32,33] and revPBE[34,35] functionals on a "test set" of several known carbonyl complexes and used the bond lengths and CO stretching frequency (ν_{CO}) to gauge the accuracy of the different functionals. Though all three functionals gave the same trends, the pure functionals BP86 and revPBE performed best in terms of agreement of the bond lengths and CO stretching frequencies with the test set. For simplicity, the BP86 results are shown here, and revPBE results are shown in the Supporting Information.

Geometry optimization of singlet (^{1}**2**) and triplet (^{3}**2**) states leads to structures that differ by spin state but are independent of the functional used. Singlet ^{1}**2** optimizes to a structure that closely approximates the crystallographic structure (Figure 7, top). The triplet ^{3}**2**, on the other hand, has a three-coordinate planar T-shaped structure in which the diketiminate reverts to its familiar κ^2 binding mode (Figure 7, bottom). This T shape

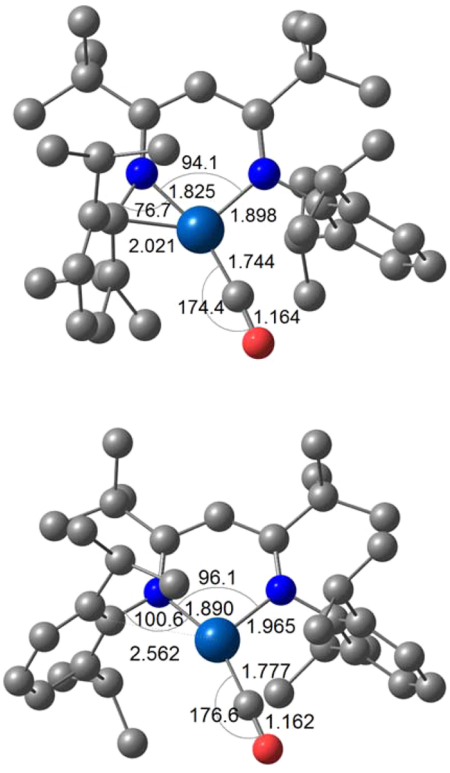

Figure 7. Optimized structures of **2** in (top) $S = 0$ (^{1}**2**) and (bottom) $S = 1$ (^{3}**2**) states using DFT calculations (BP86/def2-TZVP). Color code: C, gray; N, blue; O, red; Co, royal blue. Hydrogen atoms are omitted for clarity.

DOI: 10.1021/jacs.5b06078
J. Am. Chem. Soc. 2015, 137, 10689−10699

was previously observed in calculations on triplet $L^{trunc}Co(CO)$ using a truncated diketiminate ligand $L^{trunc} = C_3N_2H_5^-$.[36] The enthalpy of ^{3}**2** is calculated to be 5 kcal/mol higher than ^{1}**2**, which agrees well with the experimental enthalpy difference of 1−2 kcal/mol from both UV−vis and NMR data (see above). We located a minimum energy crossing point (MECP) between the two forms, which is quite close to ^{3}**2** in both energy and structure (Figure S7). This small energy difference explains the observed rapid transition between spin isomers, even though there is an unusual formation of a new bond that accompanies the spin-state change.

Table 1. Comparison of Experimental and Calculated Bond Distances (Angstroms) and Angles (degrees) for Triplet (^{3}2) and Singlet (^{1}2) $L^{tBu}Co(CO)$

	2 (crystal)	^{1}**2** (calcd)	^{3}**2** (calcd)
Co−N	1.811(1)	1.825	1.890
	1.9019(9)	1.898	1.965
$Co-C_{CO}$	1.743(1)	1.744	1.777
$Co-C_{Ar-N}$	2.041(1)	2.021	2.562
$Co-C_{Ar-iPr}$	2.221(1)	2.198	3.283
N−Co−N	94.50(4)	94.1	96.1
$Co-C_{CO}-O$	174.3(1)	174.4	176.6

The correlation between spin state and geometry at the cobalt(I) center can be rationalized from qualitative ligand field arguments (these will be supplemented below by multireference ab initio calculations). Crystalline ^{1}**2** has $S = 0$ because of its pseudo-square-planar d^8 configuration, but this comes at the expense of strain in the diketiminate ligand. This strain can be released in a three-coordinate structure that has a high-spin electronic configuration. Going in the other direction, the coordinative unsaturation of three-coordinate ^{3}**2** can be alleviated by coordinating the arene ring and gaining the ligand-field stabilization energy of the square-planar configuration but only at the expense of distorting the diketiminate ligand.

It is interesting that ^{3}**2** has a T-shaped geometry though the solution ^{1}H NMR spectrum indicates C_{2v} symmetry (see above). This averaged symmetry can be achieved through a rocking motion of the CO from side to side, through which the CO ligand samples both sides of the complex. DFT calculations indicate that the symmetric transition state for this rocking process is only ca. 10 kcal/mol above the energy of the T-shaped ground state of ^{3}**1**, consistent with the experimental inability to "freeze out" the motion in ^{1}H NMR spectra at accessible temperatures.

The T-shaped geometry of ^{3}**2** resembles those of diketiminate-supported nickel(I) monocarbonyl complexes (Figure 8). A nickel(I) carbonyl complex supported by the less bulky L^{Me} ligand features a CO stretching frequency at 2022 cm^{-1}, and its bulkier analog $L^{tBu}Ni(CO)$ exhibits a similar CO stretching frequency at 2020 cm^{-1}.[37,38] Consistent with stronger π-back-bonding from the less electronegative cobalt, **2** exhibits a lower-energy CO stretch in both the triplet and the singlet states, which agrees with the longer C−O distances. No arene interaction with the nickel(I) center exists for $L^{Me}Ni(CO)$ or $L^{tBu}Ni(CO)$ in the solid state, presumably because the d^9 electronic configuration of nickel(I) does not have as great a driving force to achieve a pseudo-square-planar conformation as in the low-spin d^8 configuration in cobalt(I).

Above, it was noted that the solid-state infrared spectrum of **2** has a CO stretching vibration at 1938 cm^{-1}, while in a THF or benzene solution of **2** the CO vibration is found at 1969 cm^{-1}. This difference is reproduced by DFT: ^{3}**2** is predicted to have a significantly higher CO stretching frequency than ^{1}**2** using each functional, and BP86 predicts a stretching frequency of 1970 cm^{-1} in excellent agreement with experiment. The structural change between ^{3}**2** and ^{1}**2** explains the lower stretching frequency of coordinated CO in ^{1}**2**. The pseudo-square-planar ^{1}**2** has no electrons in σ-antibonding orbitals, leading to a short Co−CO bond and good spatial overlap of filled d orbitals with CO π^* orbitals that gives effective back-bonding. The T-shaped geometry of ^{3}**2**, on the other hand, affords weaker M−C σ bonding and a longer M−C bond, which in turn produces less π-back-bonding.

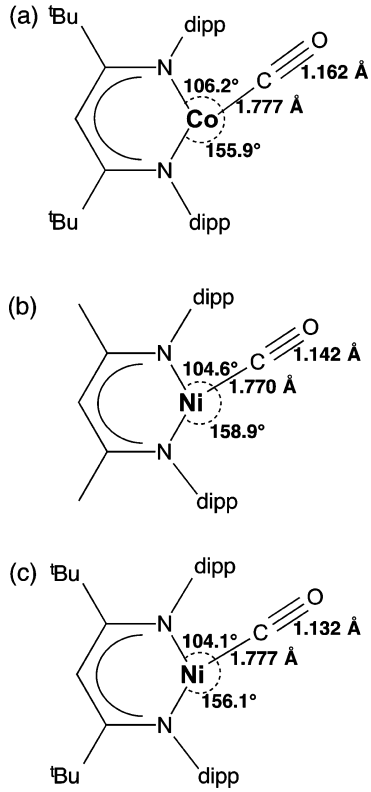

Figure 8. Calculated structural parameters of ^{3}**2** (a) compared with literature values for $L^{Me}Ni(CO)$[37] (b) and $L^{tBu}Ni(CO)$[38] (c).

Ligand Field Analysis. Ab initio calculations (CASSCF(8,5)/NEVPT2) were used for more in-depth ligand field analysis of the electronic structure of **1** (Figure 9) and **2** (Figure 10). As shown before,[17] the SOMOs of **1** are d_{xz} and d_{yz} orbitals of Co with a small admixture of nitrogen lone pair and π orbitals of coordinated Ar. The small splitting (~1500 cm^{-1}) of these orbitals is the reason that the ground state is a triplet, which is well isolated from the first singlet excited state ($\Delta E \approx 12\,000$ cm^{-1} from NEVPT2). The large separation of doubly occupied orbitals and SOMOs causes the first triplet excited state to also have a relatively high energy (~10 000 cm^{-1}).

Addition of the CO ligand (going from **1** to **2**) dramatically changes both the geometric and the electronic structure of the complex. As discussed above, there are two stable geometries, which correspond to the triplet ^{3}**2** and singlet ^{1}**2** states. The structural differences between ^{1}**2** and ^{3}**2** cause an almost 2-fold larger overall splitting of d orbitals in ^{1}**2** than in ^{3}**2** (Figure 10). The main reason is a strong antibonding interaction with the

DOI: 10.1021/jacs.5b06078
J. Am. Chem. Soc. 2015, 137, 10689−10699

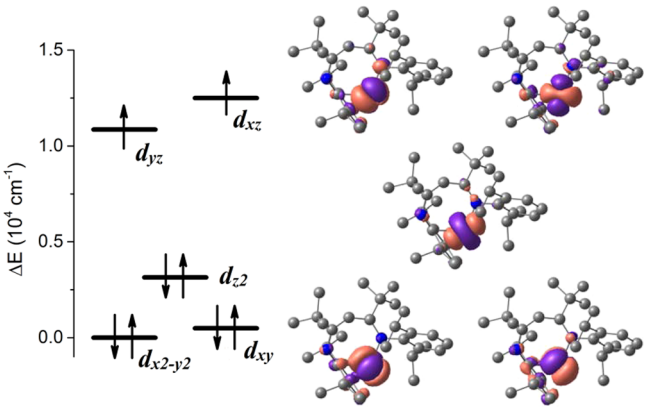

Figure 9. Energies and wave functions of d orbitals of **1** from ab initio ligand field analysis based on CASSCF(8,5)/NEVPT2 calculations. Assignment of the orbitals is in the basis where the z axis is along the Co−Ar bond and the x axis is in the Ar_{center}−Co−N_{coord} plane.

bound aryl ring in ^{1}**2** that pushes the $d_{x^2-y^2}$ orbital high in energy, so the first excited triplet state is only ∼5000 cm^{-1} above the ground singlet state (see Supporting Information for energies of the excited states). In both structures, the $d_{x^2-y^2}$ orbital also has strong antibonding interactions with the β-diketiminate ligand, because of the bite angle near 90°. In this respect, the d-orbital splitting in ^{1}**2** is much like that for a square-planar geometry. However, since the CO ligand is close to the x axis, π-back-bonding with the CO ligand stabilizes the d_{xz} orbital much more than the d_{yz} orbital, splitting them by ∼5000 cm^{-1}. The interaction with π_y*(CO) also stabilizes the d_{xy} orbital. As a result, the interplay of antibonding interaction with the β-diketiminate ligand and π-back-bonding with the CO ligand leads to an unusual quasi-degeneracy of d_{yz} and d_{z^2} orbitals. In ^{3}**2** these two orbitals have different numbers of electrons, suggesting the presence of a near degenerate orbital ground state (indeed, the first excited state is only ∼700 cm^{-1} higher in energy), which gives rise to the observed highly anisotropic magnetism of ^{3}**2** (see below).

Magnetic Properties of 1 and ^{3}2, and Exceptionally Large Zero-Field Splitting in ^{3}2. High-spin cobalt(I) complexes are much less common than low-spin, square-planar cobalt(I) complexes.[39] Pseudo-tetrahedral cobalt(I) complexes can be high spin and typically have positive zero-field splitting on the order of 1−10 cm^{-1}.[40] However, there are some examples of two-coordinated Co(I) complexes with quite large zero-field splitting.[41−43]

The analysis of variable-temperature, variable-field (VTVH) magnetization of the powder sample of **1** and the frozen eicosane solution of **2** with a sufficient fraction of ^{3}**2** reveals large magnetic anisotropy in both cases, although the sign of the zero-field splitting is different. Global fitting of the temperature dependence of the magnetic susceptibility data together with variable-field magnetization curves recorded at 1, 4, and 7 T by using an effective spin-Hamiltonian of the form $\hat{H} = D(\hat{S}_z^2 - (\hat{S}^2/3) + (E/D)(\hat{S}_x^2 - \hat{S}_y^2)) + g_{\parallel}\beta H_z\hat{S}_z + g_{\perp}\beta H_{\perp}(\hat{S}_x + \hat{S}_y)$ gives excellent global fits in both cases (Figure 11).

The best fit spin Hamiltonian parameters indicate easy *plane* anisotropy of the g tensor in **1** and easy *axis* anisotropy in ^{3}**2**. The positive sign of D in **1** shows that the diamagnetic $M_S = 0$ sublevel is the lowest in energy, and the mixing of $M_S = \pm 1$ is small ($E/D = 0.05$). In contrast, ^{3}**2** has almost uniaxial negative zero-field splitting which is extremely large (Table 2).

The origin of the large zero-field splitting in both cases is strong spin−orbit coupling with low-lying excited states; the spin−spin dipolar contribution is two orders magnitude smaller

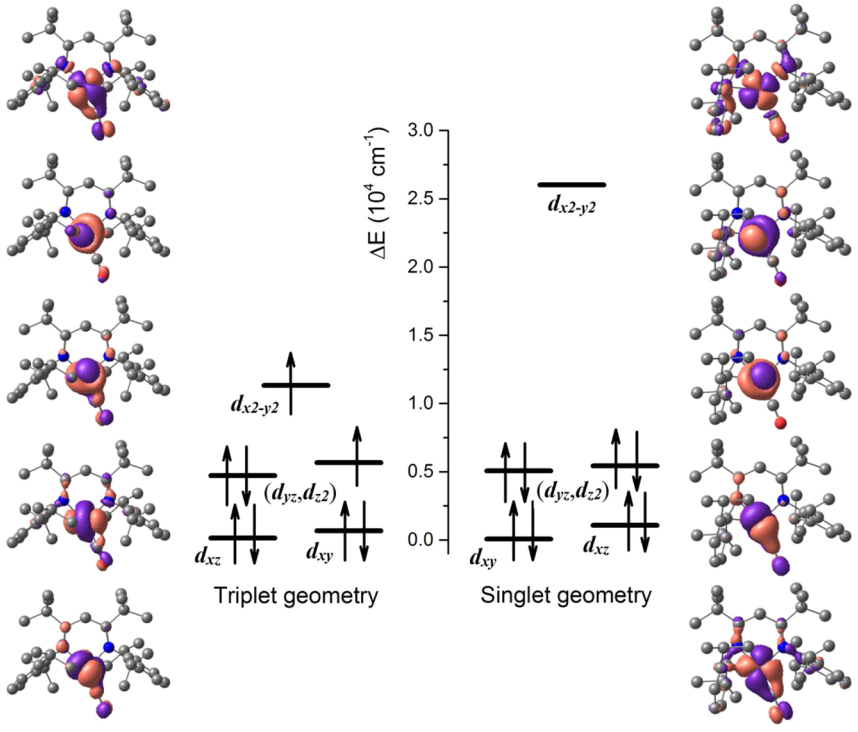

Figure 10. Energies and wave functions of d orbitals of ^{3}**2** (left) and ^{1}**2** (right) from ab initio ligand field analysis based on CASSCF(8,5)/NEVPT2 calculations. Labeling of the orbitals is approximate and corresponds to the z axis perpendicular to the β-diketiminate ligand and x axis along the Co−CO bond.

DOI: 10.1021/jacs.5b06078
J. Am. Chem. Soc. 2015, 137, 10689−10699

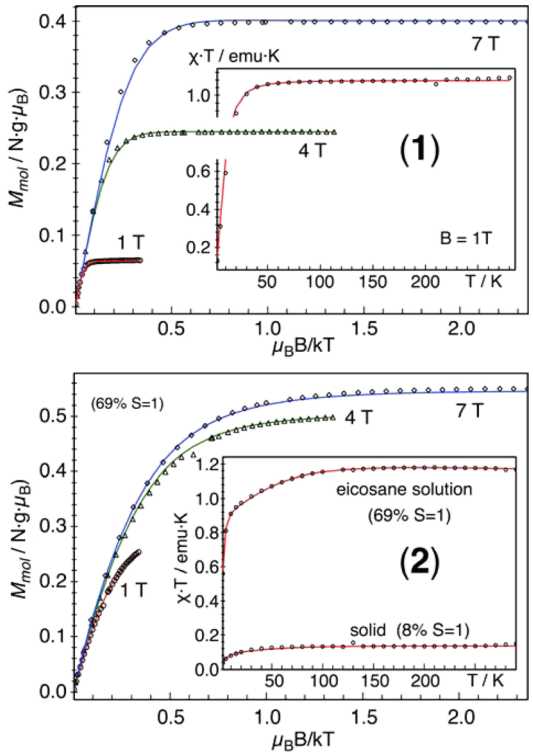

Figure 11. Field-dependent magnetization data of a solid powder sample of **1** (top) and **2** in frozen eicosane solution (bottom). (Insets) Corresponding susceptibility data recorded with B = 1 T; in the bottom inset the powder data for **2** are also included. Colored lines are the result of global simulations for S = 1 with spin Hamiltonian parameters given in Table 2.

Table 2. Spin Hamiltonian Parameters Extracted from the Fitting of VTVH Magnetization Experiments and Values Computed with the SOC-CASSCF(8,5)/NEVPT2 Method Using the Effective Hamiltonian Approach[a]

compound	D, cm^{-1}	E/D	$g_\perp$	$g_\parallel$
	fitting of the experimental data			
1	21	0.05	2.094	2.037
^{3}**2**	−150	0.011	2.136	3.240
	CASSCF(8,5)/NEVPT2			
1	28	0.05	2.238/2.210	2.003
^{3}**2**	−191	0.007	1.921/1.999	3.460

[a]The calculations for **1** are based on the crystal structure, whereas for ^{3}**2** the truncated BP86-optimized structure was used.

than SOC (~0.1 cm^{-1} estimated by DFT). Analysis of SOC-CASSCF(8,5)/NEVPT2 calculations[44] shows that the zero-field splitting of **1** has two dominant positive contributions, from two low-lying triplet states at 9000 and 10 000 cm^{-1}. There are some significant (~5 cm^{-1}) contributions from singlet states, but they cancel each other (Table S3). The zero-field splitting of ^{3}**2** is dominated by a single contribution of −230 cm^{-1} from the lowest triplet excited state at ~700 cm^{-1} (contributions from other triplet and singlet states are only ~10 cm^{-1} and slightly reduce the absolute value of total D). The computations show that d_{yz} and d_{z^2} orbitals are quasi-degenerate, such that the one-electron excitation from d_{yz} to d_{z^2} is energetically easy (Figure 10, left). The corresponding spin−orbit coupling contribution yields an easy magnetization along the x axis and large negative zero-field splitting, as found also in three-coordinate iron(II) complexes.[45] Indeed, the calculated direction of the easy axes of D and g tensors are almost collinear with the Co−CO bond.

Relationship to Other Binding Modes of β-Diketiminates, and Mechanism of Interconversion. The starting material for these reactions is L^{tBu}Co (**1**), which has κ^1,η^6 binding of the diketiminate ligand to the cobalt(I) center and one of the two nitrogen atoms.[17] Coordination of Lewis bases caused rapid rearrangement to a κ^2 binding mode (Scheme 1 above). Kinetic studies on the reaction with pyridines showed that ligand binding to the Co center in L^{tBu}Co preceded any rate-limiting rearrangement of the ligand, but the nature of the bonding in these intermediates was unclear. Particularly mysterious was how the diketiminate moves from arene binding to N binding.

The κ^1,η^2 binding mode observed in the new crystal structure of L^{tBu}Co(CO) is thus significant because it lies partway between the κ^2 and the κ^1,η^6 binding modes. Starting from L^{tBu}Co, the second nitrogen has coordinated and the arene has two rather than six carbon atoms within bonding distance of the cobalt(I) center. This structure suggests that the "hemilabile" nature of the diketiminate in L^{tBu}Co could involve the Co atom sliding along the NC_6 face of the diketiminate ligand.

Computations reveal a low-energy pathway for CO binding that proceeds in two steps (Figure 12, top). The first step is

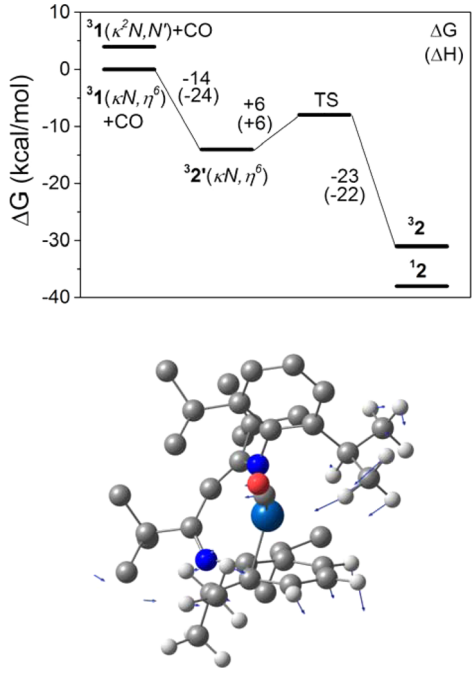

Figure 12. (Top) Calculated potential energy surface for conversion of ^{3}**1** to ^{3}**2** upon addition of CO. **2′** represents a transient CO complex in which the arene has not yet "slipped" from η^6 to η^2 binding. (Bottom) Transition state "TS" showing the imaginary frequency that corresponds to the reaction coordinate.

barrierless binding of CO to **1**, which causes minimal structural changes to the supporting ligand during exothermic and exergonic formation of a first CO adduct ^{3}**2′**. The second step is isomerization of the supporting ligand, where the Co−Ar bond is broken and the Co−N bond is formed. In the transition state for this process, the cobalt atom has slid along the arene toward the nitrogen atom and the reaction coordinate is shortening the Co−N distance and moving the coordinated

DOI: 10.1021/jacs.5b06078
J. Am. Chem. Soc. 2015, 137, 10689−10699

arene away from cobalt (Figure 12, bottom). A scan of the electronic energy as a function of the Co−N bond length (with full geometry optimization of all other parameters) shows that the gain and loss of bonding energy is almost perfectly in balance during this sliding motion, such that the activation barrier for the second step is only 6 kcal/mol. Interestingly, in the transition state one isopropyl group of the uncoordinated arene has a methyl C−H bond very close to the cobalt center (Co−H distance = 2.4 Å), and this isopropyl group is moving in the imaginary frequency (Figure 12, bottom). We surmise that this C−H bond plays a role in stabilizing the transition state for this isomerization by fulfilling some of the electronic need of the cobalt center during the part of the reaction when the Co−N and Co−arene bonding are partially disrupted.

In order to explore the generality of this sliding motion to other examples of diketiminate hemilability, we also performed DFT calculations on the approach of pyridine to $L^{tBu}Co$ to form $L^{tBu}Co(py)$, a reaction that we previously studied using kinetics.[17] In this case, the initial adduct corresponding to **2′** above (Figure S12) is roughly thermoneutral with $L^{tBu}Co$ and pyridine and again has low barriers toward either $L^{tBu}Co$ + py or toward the experimentally observed κ^2-bound, three-coordinate $L^{tBu}Co$(pyridine) complex. A constrained scan that varies the different Co−N distances (but optimizes other atomic positions) is displayed in Table S7 and animated in Figure S14. After weak pyridine association, the losses and gains in energy are roughly equal as the Co moves across the arene from η^6 to η^1 (bound to the ipso carbon), and then the major stabilization occurs when the strain in the diketiminate ring is released concomitant with $Co-N_{diketiminate}$ bond formation. No agostic interactions are evident in this case, presumably because of the greater size of the pyridine ligand. Overall, the calculations on both CO and pyridine binding demonstrate that the diketiminate slides along the N−C and C−C bonds smoothly between binding modes during coordination of the added ligand.

DISCUSSION

Spin crossover during the reactions of high-spin complexes is a phenomenon of great current interest.[21,46−51] Complex **2** undergoes rapid spin crossover between the solid state (predominantly singlet ^{1}**2** with S = 0) and solution (predominantly triplet ^{3}**2** with S = 1), as shown by changes in color, magnetic susceptibility, and ^{1}H NMR spectra that are rapid (within time of mixing). All solvents that were tested (pentane, benzene, THF) gave the triplet form in solution, and an increasing amount of singlet appeared at low temperatures. All of the data presented above fit a spin equilibrium model in which the S = 1 spin state is 1−2 kcal/mol higher in enthalpy than the S = 0 spin state.

DFT computations provide a structural basis for the spin state change in **2**. The calculated CO stretching frequencies for the singlet and triplet spin states agree well with experimental solid and solution CO stretching frequencies, respectively. Singlet **2** is calculated to be close in energy relative to triplet **2**, consistent with the difference of 1−2 kcal/mol from analysis of ^{1}H NMR and UV−vis data. Most importantly, the DFT calculations elucidate the structure of the solution triplet form, which is three coordinate and T shaped. This differs from the singlet form, in which the geometry is pseudo-square planar because a C−C bond of a ligand arene forms a bond to the cobalt(I) center. There is clearly a delicate balance of strain energy, back-bonding, and coordination number that determines the geometry and spin state (Figure 13).

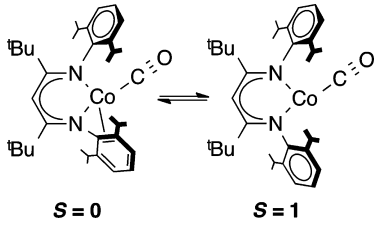

Figure 13. Correlation between coordination number and spin state in the spin isomers of $L^{tBu}Co(CO)$ (**2**).

The singlet and triplet forms of $L^{tBu}Co(CO)$ interconvert on the NMR time scale even at low temperature, and thus, the barrier to spin crossover is extremely low. We have seen that barriers for spin-state crossover during β-hydride elimination from cobalt(II) or iron(II) complexes are negligible at the minimum energy crossing point along the potential energy surface of a given spin state.[52] There are cobalt(II) systems in which coordination induces a spin-state change.[53] However, ligand-induced spin-state crossover is rare for cobalt(I) systems and highlights the ability of the β-diketiminate ligand to facilitate access to multiple spin states at the metal center by providing flexible support.

The spin crossover in $L^{tBu}Co(CO)$ is different than those that have been studied for other complexes in two ways. First, there is the formation/cleavage of bonds during this transition. Despite the change in bonding, we consider this a "true" spin crossover because the change in population as a function of temperature (in the solution state) fits well to standard models.[25−27] Second, the interconversion of spin isomers occurs only in solution; SQUID magnetometry of solid samples does not show any signs of spin crossover. It is likely that the constraints of the crystal lattice prevent the formation of ^{3}**2** from ^{1}**2** in the crystal.

It is also interesting that the paramagnetic form ^{3}**2** has exceptionally large easy-axis zero-field splitting with D of ca. −150 cm^{-1}. This highly anisotropic magnetism is characteristic of single-molecule magnets, where the magnitude of $-D$ is proportional to the barrier for magnetic reversal.[54] Normally, such large magnetic anisotropy requires highly symmetric environments, which have a nearly degenerate ground state as reported recently for linear d^8 complexes.[55,56] It is therefore interesting that a similarly low-lying excited state can be achieved in this lower-symmetry system that is more amenable to steric and electronic tuning. Thus, ^{3}**2** has promise for further exploration of its magnetic properties.

CONCLUSIONS

A novel low-coordinate cobalt(I) compound has a β-diketiminate ligand with an unprecedented and highly strained κ^1,η^2 coordination mode. Thus, this complex shows the versatility and flexibility of β-diketiminate supporting ligands, which can slide between κ^1,η^6 and κ^2 binding modes with low barriers despite significant ligand rearrangement. The change in geometry at the cobalt center in $L^{tBu}Co(CO)$ is accompanied by a rapid, reversible spin-state change. A combination of magnetic, spectroscopic, structural, and computational studies elucidates the nature of this spin-state crossover and shows that the high-spin form has highly anisotropic magnetism and nearly

DOI: 10.1021/jacs.5b06078
J. Am. Chem. Soc. 2015, 137, 10689−10699

axial zero-field splitting due to near degeneracy of filled and half-filled d orbitals. These results offer new strategies, both for creation of reactive low-coordinate sites for catalysis and for magnetic switching in molecular materials.

EXPERIMENTAL SECTION

General Considerations. All manipulations were performed under an argon atmosphere using standard Schlenk techniques or in an M. Braun glovebox maintained at or below 1 ppm of O_2 and H_2O. Glassware was dried at 150 °C overnight. Hexane and toluene were purified by passage through activated alumina and "deoxygenizer" columns from Glass Contour Co. (Laguna Beach, CA). Celite was dried at 300 °C under vacuum overnight. THF was dried by distilling from Na/benzophenone. THF-d_8 was dried over CaH_2 and then over Na/benzophenone and vacuum transferred and stored over 3 Å molecular sieves. $L^{tBu}CoCl$,[57] $L^{tBu}Co$,[17] and $L^{tBu}Co(CO)_2$[17] were synthesized according to published procedures.

^1H NMR spectra were recorded on a Bruker Avance 500 MHz spectrometer. The NMR probe temperature was calibrated using methanol. IR spectra were recorded on a Shimadzu FTIR spectrophotometer (FTIR-8400S). UV−vis absorption spectra were recorded on a Cary 50 or Cary 60 spectrophotometer using Teflon-sealed quartz cuvettes. Elemental analyses were obtained from the CENTC Elemental Analysis Facility at the University of Rochester. Microanalysis samples were handled under argon and weighed with a PerkinElmer Model AD-6 Autobalance, and their compositions were determined with a PerkinElmer 2400 Series II Analyzer.

Synthesis of $L^{tBu}Co(CO)$ (2). A solution of $L^{tBu}Co$ (50 mg, 88 μmol) in THF (5 mL) was added to a vial containing a red solution of $L^{tBu}Co(CO)_2$ (55 mg, 88 μmol) in THF (5 mL). The resulting green-yellow solution was stirred for 30 min at room temperature. The solution was concentrated under vacuum to ∼5 mL and stored at −40 °C until red crystals formed (67 mg). The crystalline solid was isolated, and the supernatant was concentrated to ∼2 mL and stored at −40 °C for additional crystal formation (32 mg; total yield = 99 mg, 95%). ^1H NMR (500 MHz, C_6D_6): δ 56.8 (1H, backbone-C*H*), 18.0 (18H, *t*-Bu), 11.3 (4H, *m*-Ar), −8.1 (12H, iPr-CH_3), −39.8 (2H, iPr-C*H*), −43.2 (2H, *p*-Ar), −61.2 (12H, iPr-CH_3) ppm. μ_{eff} (C_6D_6, 25 °C): 3.3 μ_B. IR (KBr): 2953 (s), 2912 (m), 2856 (m), 1988 (w), 1938 (vs), 1544 (w), 1504 (w), 1437 (w), 1358 (m), 1308 (w), 1205 (w) cm^{-1}. IR (benzene): 3028 (m), 2962 (w), 2926 (w), 2879 (w), 1969 (s), 1938 (w), 1604 (m), 1494 (s), 1464 (m), 1390 (w), 1378 (w), 1321 (w), 1083 (w), 1030 (w) cm^{-1}. UV−vis (THF): 306 (14 $mM^{-1}cm^{-1}$), 338 (13 mM^{-1} cm^{-1}), 583 (0.4 mM^{-1} cm^{-1}) nm. Anal. Calcd for $C_{36}H_{53}N_2OCo$: C, 73.44; H, 9.07; N, 4.76. Found: C, 73.11; H, 9.08; N, 4.58.

Magnetic Measurements. Magnetic susceptibility data were measured either from powder samples of solid material or from solution in eicosane (melting point 310 K) in the temperature range 2−270 K by using a SQUID susceptometer with fields from 1 to 7 T (MPMS-7, Quantum Design, calibrated with standard palladium reference sample, error < 2%). In order to confirm that the magnetic behavior did not change with shipping to Germany, we also confirmed the room-temperature magnetic moments in Rochester on a Johnson Matthey MSB-1 magnetic susceptibility balance. Multiple-field variable-temperature magnetization measurements were done at 1, 4, and 7 T in the range 2−260 K with the magnetization equidistantly sampled on a $1/T$ temperature scale. Samples were measured in holders of quartz with O-ring seals or in flame-sealed, ca. 8 cm long pieces of 5 mm NMR tubes, which were fixed in a straw together with a similar compensation tube below the sample. Powders were fixed with quartz wool to prevent torquing. The SQUID response curves (raw data) were corrected for holder and solvent contributions by subtracting the corresponding response curves obtained from separate measurements with and without sample material. The experimental magnetization data obtained from independent simulation of the corrected SQUID response curves were corrected for underlying diamagnetism[58] by use of tabulated Pascal's constants,[59,60] as well as for temperature-independent paramagnetism (600 × 10^{-6} emu for **2**).

Handling and analyses of the SQUID raw data as well as spin Hamiltonian simulation of the susceptibility and magnetization data were done with our own package julX for exchange-coupled systems (available from E.B. by mail to ebill@gwdg.de). The simulations were based on the usual spin Hamiltonian operator for mononuclear system with spin $S = 1$

$$\hat{H} = D\left(\hat{S}_z^2 - \frac{\hat{S}^2}{3} + \frac{E}{D}(\hat{S}_x^2 - \hat{S}_y^2)\right) + g_{\parallel}\beta H_z\hat{S}_z + g_{\perp}\beta H_{\perp}(\hat{S}_x + \hat{S}_y)$$

where $g_{\parallel}$ and $g_{\perp}$ are the axial and equatorial components of the g tensor and D and E/D are the axial zero-field splitting and rhombicity parameters.

Diagonalization of the total Hamiltonian was performed with the routine ZHEEV from the LAPACK Library (available from E. B.), and magnetic moments were calculated from the eigenfunctions by using the Hellman−Feyman theorem

$$\vec{\mu}_i(\vec{B}) = -\langle\psi_i|\mathrm{d}\hat{H}/\mathrm{d}\vec{B}|\psi_i\rangle$$

The powder summations were done by using a 16-point Lebedev grid.[61,62]

Computation Details. The ORCA computational package was employed for all quantum chemical calculations.[63,64] Geometry optimization and frequency calculations were performed using the pure GGA functional BP86[30,31] with the def2-TZVP basis set[29,65,66] and the dispersion correction D3.[67] The auxiliary basis set def2-TZVP/J was used in conjunction with the resolution of identity (RI-J) approximation.[68] The geometries used for the calculations are listed in the Supporting Information.

The state-averaged complete active space self-consistent field (SA-CASSCF)[69−71] method with segmented all-electron relativistically contracted version[72] of the Ahlrichs polarized basis set def2-TZVP[29,65,66] was used for calculation of spin-free roots. The active space contains eight electrons in the five 3d orbitals of cobalt(I), where all 10 triplet and 15 singlet roots that arise from the d^8 configuration have been computed. The scalar relativistic effects were taken into account using the standard second-order Douglas−Kroll−Hess procedure.[73] The resolution of identity approximation with corresponding correlation fitting of the basis set was performed in order to speed up the calculations.[68] The additional *N*-electron valence perturbation theory to second-order (NEVPT2)[74−77] energy correction was performed on top of the CASSCF wave function.

The analysis of the d-orbital splitting was performed via ab initio ligand field theory.[78,79] The CASSCF wave functions and the NEVPT2-corrected energies of the excited states were used to reconstruct the matrix corresponding to the ligand field matrix parametrized in terms of 5 × 5 unknown one-electron ligand field matrix elements accounting for the splitting of the 3d orbitals and two more parameters for the interelectronic repulsion. In order to compute matrix elements of the spin−orbit coupling (SOC) operator the mean field approximation (SOMF) was used.[80] The energies and wave functions of all 45 magnetic sublevels of 10 triplet and 15 singlet roots were computed by diagonalization of the full matrix $\langle\Psi_I^{SM_S}|\hat{H}_{BO} + \hat{H}_{SOC}|\Psi_J^{S',M_S'}\rangle = \delta_{IJ}\delta_{SS'}\delta_{M_SM_S'}E_I^S + \langle\Psi_I^{SM_S}|\hat{H}_{SOC}|\Psi_J^{S',M_S'}\rangle$. The spin Hamiltonian parameters were evaluated using the effective Hamiltonian approach[81] where the splitting and mixing of the ground triplet magnetic sublevels are mapped to the spin Hamiltonian formalism.

ASSOCIATED CONTENT

Supporting Information

The Supporting Information is available free of charge on the ACS Publications website at DOI: 10.1021/jacs.5b06078.

Additional spectroscopic (PDF)

Additional crystallographic information (CIF)

QuickTime movie of a constrained scan of Co−N distances leading to pyridine binding to **1** (MOV)

DOI: 10.1021/jacs.5b06078
J. Am. Chem. Soc. 2015, 137, 10689−10699

AUTHOR INFORMATION

Corresponding Author

*patrick.holland@yale.edu

Notes

The authors declare no competing financial interest.

ACKNOWLEDGMENTS

The authors acknowledge financial support by the Max Planck Society, Yale University, and the U.S. Department of Energy, Office of Basic Energy Sciences, grant DE-FG02-09ER16089. Analytical data were obtained from the CENTC Elemental Analysis Facility at the University of Rochester, funded by NSF grant CHE-0650456. The computations were supported in part by the facilities and staff of the Yale University Faculty of Arts and Sciences High Performance Computing Center and by the National Science Foundation under grant CNS-0821132 that partially funded acquisition of the facilities.

REFERENCES

(1) Jeffrey, J. C.; Rauchfuss, T. B. *Inorg. Chem.* **1979**, *18*, 2658.
(2) Bassetti, M. *Eur. J. Inorg. Chem.* **2006**, *2006*, 4473.
(3) Annibale, V. T.; Song, D. *RSC Adv.* **2013**, *3*, 11432.
(4) Braunstein, P.; Naud, F. *Angew. Chem., Int. Ed.* **2001**, *40*, 680.
(5) Jiménez, M. V.; Pérez-Torrente, J. J.; Bartolomé, M. I.; Gierz, V.; Lahoz, F. J.; Oro, L. A. *Organometallics* **2008**, *27*, 224.
(6) Weng, Z.; Teo, S.; Hor, T. S. A. *Acc. Chem. Res.* **2007**, *40*, 676.
(7) Wu, F.; Dioumaev, V. K.; Szalda, D. J.; Hanson, J.; Bullock, R. M. *Organometallics* **2007**, *26*, 5079.
(8) Poli, R. *Chem. Rev.* **1996**, *96*, 2135.
(9) Schröder, D.; Shaik, S.; Schwarz, H. *Acc. Chem. Res.* **2000**, *33*, 139.
(10) Poli, R.; Harvey, J. N. *Chem. Soc. Rev.* **2003**, *32*, 1.
(11) Holland, P. L. *Acc. Chem. Res.* **2015**, *48*, 1696.
(12) Smith, K. M.; Poli, R.; Legzdins, P. *Chem. - Eur. J.* **1999**, *5*, 1598.
(13) Janse van Rensburg, W.; Grové, C.; Steynberg, J. P.; Stark, K. B.; Huyser, J. J.; Steynberg, P. J. *Organometallics* **2004**, *23*, 1207.
(14) Hardman, N. J.; Fang, X.; Scott, B. L.; Wright, R. J.; Martin, R. L.; Kubas, G. J. *Inorg. Chem.* **2005**, *44*, 8306.
(15) Yang, Y.; Liu, Z.; Cheng, R.; He, X.; Liu, B. *Organometallics* **2014**, *33*, 2599.
(16) Paretzki, A.; Hubner, R.; Ye, S.; Bubrin, M.; Kamper, S.; Kaim, W. *J. Mater. Chem. C* **2015**, *3*, 4801.
(17) Dugan, T. R.; Sun, X.; Rybak-Akimova, E. V.; Olatunji-Ojo, O.; Cundari, T. R.; Holland, P. L. *J. Am. Chem. Soc.* **2011**, *133*, 12418.
(18) Dugan, T. R.; Goldberg, J. M.; Brennessel, W. W.; Holland, P. L. *Organometallics* **2012**, *31*, 1349.
(19) Strickland, N.; Harvey, J. N. *J. Phys. Chem. B* **2007**, *111*, 841.
(20) Holzhacker, C.; Standfest-Hauser, C. M.; Puchberger, M.; Mereiter, K.; Veiros, L. F.; Calhorda, M. J.; Carvalho, M. D.; Ferreira, L. P.; Godinho, M.; Hartl, F.; Kirchner, K. *Organometallics* **2011**, *30*, 6587.
(21) Lomont, J. P.; Nguyen, S. C.; Harris, C. B. *Acc. Chem. Res.* **2014**, *47*, 1634.
(22) Allen, F. H.; Bellard, S.; Brice, M. D.; Cartwright, B. A.; Doubleday, A.; Higgs, H.; Hummelink, T.; Hummelinkpeters, B. G.; Kennard, O.; Motherwell, W. D. S.; Rodgers, J. R.; Watson, D. G. *Acta Crystallogr., Sect. B: Struct. Crystallogr. Cryst. Chem.* **1979**, *35*, 2331.
(23) Ming, L.-J. In *Physical Methods in Bioinorganic Chemistry*; Que, L., Ed.; University Science Books: Sausalito, CA, 2000.
(24) Schubert, E. M. *J. Chem. Educ.* **1992**, *69*, 62.
(25) Kahn, O. *Molecular Magnetism*; Wiley-VCH: New York, 1993.
(26) Schweinfurth, D.; Demeshko, S.; Hohloch, S.; Steinmetz, M.; Brandenburg, J. G.; Dechert, S.; Meyer, F.; Grimme, S.; Sarkar, B. *Inorg. Chem.* **2014**, *53*, 8203.
(27) Gütlich, P.; Goodwin, H. A. *Top. Curr. Chem.* **2004**, *233*, 1.
(28) The ΔH values are expected to be lower than in solids, because cooperativity in solids may contribute considerably to ΔH.
(29) Weigend, F.; Ahlrichs, R. *Phys. Chem. Chem. Phys.* **2005**, *7*, 3297.
(30) Becke, A. D. *Phys. Rev. A: At., Mol., Opt. Phys.* **1988**, *38*, 3098.
(31) Perdew, J. P. *Phys. Rev. B: Condens. Matter Mater. Phys.* **1986**, *33*, 8822.
(32) Lee, C. T.; Yang, W. T.; Parr, R. G. *Phys. Rev. B: Condens. Matter Mater. Phys.* **1988**, *37*, 785.
(33) Becke, A. D. *J. Chem. Phys.* **1993**, *98*, 1372.
(34) Perdew, J. P.; Burke, K.; Ernzerhof, M. *Phys. Rev. Lett.* **1996**, *77*, 3865.
(35) Zhang, Y. K.; Yang, W. T. *Phys. Rev. Lett.* **1998**, *80*, 890.
(36) Liu, C.; Cundari, T. R.; Wilson, A. K. *J. Phys. Chem. C* **2012**, *116*, 5681.
(37) Eckert, N. A.; Dinescu, A.; Cundari, T. R.; Holland, P. L. *Inorg. Chem.* **2005**, *44*, 7702.
(38) Horn, B.; Pfirrmann, S.; Limberg, C.; Herwig, C.; Braun, B.; Mebs, S.; Metzinger, R. *Z. Anorg. Allg. Chem.* **2011**, *637*, 1169.
(39) Cotton, F. A.; Wilkinson, G.; Murillo, C. A.; Bochmann, M. *Advanced Inorganic Chemistry*, 6th ed.; John Wiley & Sons, Inc.: New York, 1999.
(40) Krzystek, J.; Ozarowski, A.; Zvyagin, S. A.; Telser, J. *Inorg. Chem.* **2012**, *51*, 4954.
(41) Ohare, D.; Raichaudhuri, A.; Murphy, V. *J. Chem. Soc., Dalton Trans.* **1993**, 3071.
(42) Lin, C. Y.; Fettinger, J. C.; Grandjean, F.; Long, G. J.; Power, P. P. *Inorg. Chem.* **2014**, *53*, 9400.
(43) Zhao, P.; Brown, Z.; Fettinger, J. C.; Grandjean, F.; Long, G. J.; Power, P. P. *Organometallics* **2014**, *33*, 1917.
(44) Atanasov, M.; Aravena, D.; Suturina, E.; Bill, E.; Maganas, D.; Neese, F. *Coord. Chem. Rev.* **2015**, *289−290*, 177.
(45) Andres, H.; Bominaar, E.; Smith, J. M.; Eckert, N. A.; Holland, P. L.; Münck, E. *J. Am. Chem. Soc.* **2002**, *124*, 3012.
(46) Keogh, D. W.; Poli, R. *J. Am. Chem. Soc.* **1997**, *119*, 2516.
(47) Hirsekorn, K. F.; Hulley, E. B.; Wolczanski, P. T.; Cundari, T. R. *J. Am. Chem. Soc.* **2008**, *130*, 1183.
(48) Renz, A. L.; Pérez, L. M.; Hall, M. B. *Organometallics* **2011**, *30*, 6365.
(49) Maestre, L.; Sameera, W. M. C.; Díaz-Requejo, M. M.; Maseras, F.; Pérez, P. J. *J. Am. Chem. Soc.* **2013**, *135*, 1338.
(50) Usharani, D.; Janardanan, D.; Li, C.; Shaik, S. *Acc. Chem. Res.* **2013**, *46*, 471.
(51) Saouma, C. T.; Mayer, J. M. *Chem. Sci.* **2014**, *5*, 21.
(52) Bellows, S. M.; Cundari, T. R.; Holland, P. L. *Organometallics* **2013**, *32*, 4741.
(53) Heinze, K.; Huttner, G.; Zsolnai, L.; Schober, P. *Inorg. Chem.* **1997**, *36*, 5457.
(54) Murrie, M. *Chem. Soc. Rev.* **2010**, *39*, 1986.
(55) Lin, C.-Y.; Fettinger, J. C.; Grandjean, F.; Long, G. J.; Power, P. P. *Inorg. Chem.* **2014**, *53*, 9400.
(56) Lin, C.-Y.; Guo, J.-D.; Fettinger, J. C.; Nagase, S.; Grandjean, F.; Long, G. J.; Chilton, N. F.; Power, P. P. *Inorg. Chem.* **2013**, *52*, 13584.
(57) Ding, K.; Holland, P. L.; Adhikari, D.; Mindiola, D. J. *Inorg. Synth.* **2010**, *35*, 43.
(58) Bain, G. A.; Berry, J. F. *J. Chem. Educ.* **2008**, *85*, 532.
(59) O'Connor, C. J. *Prog. Inorg. Chem.* **1982**, *29*, 203.
(60) Weast, R. C.; Astle, M. J. *CRC Handbook of Chemistry and Physics*; CRC Press Inc.: Boca Raton, FL, 1979.
(61) Lebedev, V. I.; Laikov, D. N. *Dokl. Math.* **1999**, *59*, 477.
(62) A Fortran code to generate Lebedev grids up to order $L = 131$ is available at http://server.ccl.net/cca/software/SOURCES/.
(63) Neese, F. *Wires Comput. Mol. Sci.* **2012**, *2*, 73.
(64) Neese, F. *Wiley Interdisciplinary Reviews: Computational Molecular Science* **2012**, *2*, 73−78.
(65) Schäfer, A.; Huber, C.; Ahlrichs, R. *J. Chem. Phys.* **1994**, *100*, 5829.
(66) Schäfer, A.; Horn, H.; Ahlrichs, R. *J. Chem. Phys.* **1992**, *97*, 2571.
(67) Grimme, S.; Antony, J.; Ehrlich, S.; Krieg, H. *J. Chem. Phys.* **2010**, *132*, 154104.

DOI: 10.1021/jacs.5b06078
J. Am. Chem. Soc. 2015, 137, 10689−10699

(68) Neese, F. *J. Comput. Chem.* **2003**, *24*, 1740.
(69) Roos, B. O.; Taylor, P. R.; Siegbahn, P. E. M. *Chem. Phys.* **1980**, *48*, 157.
(70) Siegbahn, P.; Heiberg, A.; Roos, B.; Levy, B. *Phys. Scr.* **1980**, *21*, 323.
(71) Siegbahn, P. E. M.; Almlof, J.; Heiberg, A.; Roos, B. O. *J. Chem. Phys.* **1981**, *74*, 2384.
(72) Pantazis, D. A.; Chen, X. Y.; Landis, C. R.; Neese, F. *J. Chem. Theory Comput.* **2008**, *4*, 908.
(73) Hess, B. A. *Phys. Rev. A: At., Mol., Opt. Phys.* **1986**, *33*, 3742.
(74) Angeli, C.; Cimiraglia, R.; Malrieu, J.-P. *Chem. Phys. Lett.* **2001**, *350*, 297.
(75) Angeli, C.; Cimiraglia, R.; Malrieu, J.-P. *J. Chem. Phys.* **2002**, *117*, 9138.
(76) Angeli, C.; Cimiraglia, R.; Evangelisti, S.; Leininger, T.; Malrieu, J.-P. *J. Chem. Phys.* **2001**, *114*, 10252.
(77) Angeli, C.; Cimiraglia, R. *Theor. Chem. Acc.* **2002**, *107*, 313.
(78) Atanasov, M.; Ganyushin, D.; Sivalingam, K.; Neese, F. *Struct. Bonding (Berlin)* **2011**, *143*, 149.
(79) Atanasov, M.; Zadrozny, J. M.; Long, J. R.; Neese, F. *Chem. Sci.* **2013**, *4*, 139.
(80) Ganyushin, D.; Neese, F. *J. Chem. Phys.* **2013**, *138*, 104113.
(81) Vallet, V.; Maron, L.; Teichteil, C.; Flament, J.-P. *J. Chem. Phys.* **2000**, *113*, 1391.

DOI: 10.1021/jacs.5b06078
J. Am. Chem. Soc. 2015, 137, 10689−10699